OPTICAL PATHLENGTH CONTROL EXPERIMENT ON JPL PHASE B TESTBED

Zahidu M. Rahman*, John T. Spanos†, John O'Brien* and Chengchin Chu†
Jet Propulsion Laboratory
California Institute of Technology
Pasadena, California 91109

1. Abstract

An experimental implementation of a nanometer level optical pathlength control for large baseline space interferometry is presented. The pathlength compensation system is installed on a large flexible experimental truss, thus structural motions play a dominant role in the control system design. The associated control structure interaction) problem is addressed to maintain the optical pathlength within the prescribed variation of 10-15 nanometer rms. By a successful blend of' a structural control for damping augmentation anda direct pathlengt h control for the pathlength compensation, the optical pathlength variation has been maintained within 6 nanometer rms under the laboratory ambient disturbance and within 9 nanometer rms under a severe forced resonant disturbance.

2. Introduction

The next generation space based astronomical missions will require large base'lillc optical interferometry for higher angular resolution and sensitivity. Figure 1. shows one possible configuration in which any two of the six collectors forms a large baseline interferometer. The astronomic accuracy of such interferometer improves with larger baseline. For the interferometer to perform its mission successfully, the variations in the length of the paths traveled by light through the pair of collectors to the detector must be no more than 15 nanometer rms [1]. An additional requirement is to maintain the wave front tilt of the traveling light within few micro-radians rms [1]. The complexity of achieving and maintaining these stringent requirements increases as collectors are mounted on large flexible structures. Also a longer baseline usually Inc'ails a more flexible mounting structure that results in a more severe interaction between the structure and the feedback control system for pathlength compensation. As a result, Control Structure Interaction (CSI) becomes an important issue in designing any compensator for the optical pathlength control.

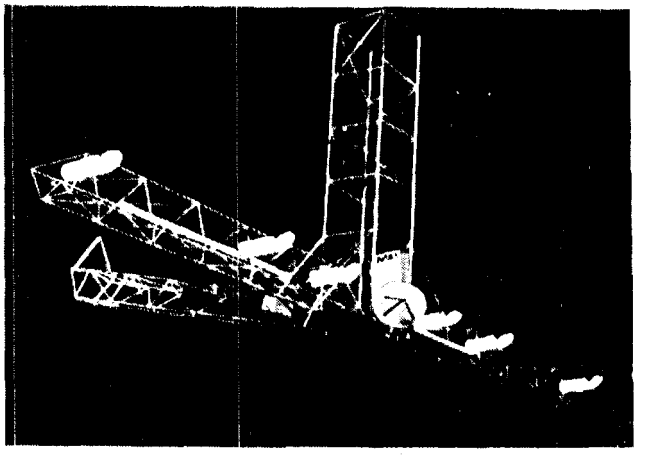

Figure 1: Focus Mission Interferometer[1]

In an experiment performed by O'Neal and Spanos[2] at the Jet Propulsion Laboratory (JPL), the optical pathlength was effectively controlled to 3 nanometer(rms). The experiment used an optical configuration that isolated structural motion from the optical path. The target mirror in the configuration was placed on a rigid frame which was unrealistic. for an actual space mission. In a separate experiment by the authors [3,.4], the target mirror was placed on the flexible testbed along with the compensation system. They observed a large cou-

*Member Technical Staff, Applied Mechanics Technologies Section

†Member Technical Staff, Guidance and Control Section

pling of strut.tura] motion to the optical pathlength and were able to control the optical pathlength to approximately 5 nanometer rms. In the setup, the target mirror and the actuators of the pathlength compensation system were placed in such a way that it effectively formed a co-located sensor and act ua - tor system. All the structural modes were interacting stably with a lead type control as expected of any co-located system. However few local modes at higher frequencies caused loss of the co-location and limited the bandwidth of the control loops.

We present results of a pathlength control experiment on the phase B testbed with a new optical setup (option 2 optics) which couples noncolocated structural motions in the optical path. The sen - sor (the target mirror) and the actuators are placed in a noncolocated fashion and the travelling light is bouncing off from two flexible booms at the top of the testbed. In this setup, the direct optical pathlength control alone is not sufficient to achieve the required performance level of the pathlength variation due to the fact that the dominant presence of the lightly damped noncolocated structural modes at low frequencies (well within the desired optical controller bandwidth) severely limits the bandwidth of the controller. Damping of selected structural modes is enhanced by implementing a structural control layer which enables a high bandwidth controller for the direct pathlength compensation. The controller maintains the pathlength variation within 6 nanometers rms when only the laboratory ambient disturbance is present and within 9 nanometers rms when a forced resonant disturbance is induced.

3. JPL Phase B Testbed

To address the control structure interaction (CSI) issue associated with the! optical pathlength co I - trol, the Jet Propulsion Laboratory has developed a ground testbed facility known as the JPL Phase B testbed (figure 2). A detailed description of the testbed is available in reference [5]. The testbed is an eight foot tall truss structure cantilevered at the base and equipped with an optical motion compensation system.

The optical element on the testbed represents a delay line for optical pathlength compensation for a stellar interferometer telescope. The direct pathlength control (also known as optical delay line control) with laser trace to simulate star light is shown in figure 2. The delay line is equipped with a pri-

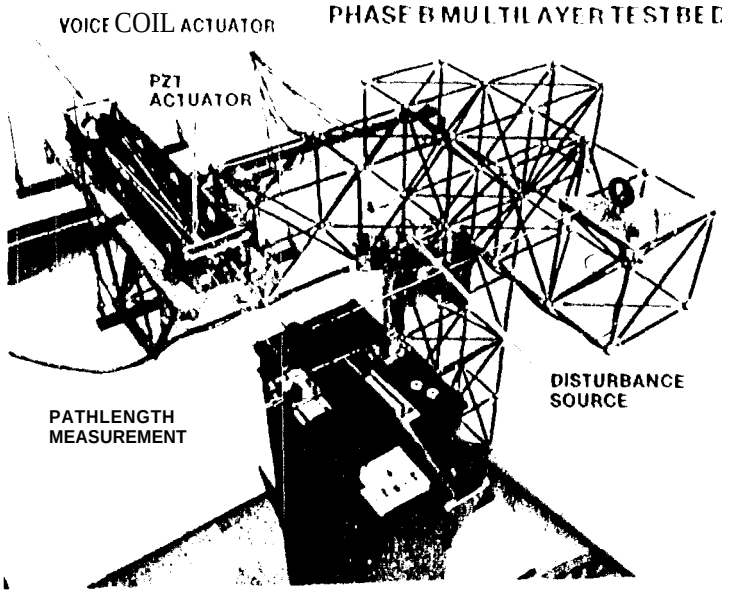

Figure 2: JPL Phase B Testbed with optical delay-line and option 2 optics. Laser simulates starlight

mary parabolic mirror and a secondary plane mirror placed at the focal point of the primary mirror. The whole mirror setup is rigidly mi-caged in an aluminum trolley suspended from the structure with soft flexures. The secondary mirror is driven relative to the trolley by a balanced PZT (piezoelectric) actuator for fine pathlength adjustment and the whole trolley is driven by a voice coil actuator for coarse pathlength compensation. The optical behavior of the setup is more like a retroreflector with a capability of providing coarse (millimeter) to very fiat (nanometer) pathlength compensation over a wide frequency bandwidth. Since the delay line compensation system and the target retroreflector are installed (figure 2) on the truss booms along X and Y directions respectively, the motion of the latter boom causes the loss of act uator-sensor co-location. We call this optical setup as option 2 optics on Phase B testbed Structure,

In the pathlength compensation system, Retroreflector and Plane Mirror Interferometry are combined such that the optical alignment is maintained under translational and rotational motions. This optical configuration, as compared to retroreflector interferometry or plane mirror interferometry, is less likely to lose its alignment due to the structural vibration. The laser beam passes eight times through the trol-

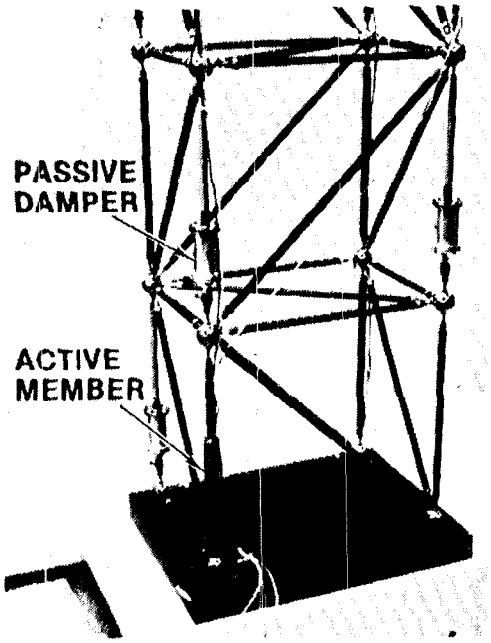

Figure 3: Active and passive dampers embedded into JPL Phase B Testbed

ley, as compared to two times in retroreflector interferometry or four times in plane mirror interferometry, resulting in an enhanced laser metric resolution.

The testbed is also embedded with four passive Honeywell viscous dampers [12] and four piezoelectric active members for structural control to augment modal damping (figure 3). The stiffness and the damping coefficient of the passive dampers are fixed ie, can not be altered. However these properties of the active members can be tuned through feedback loops. For this purpose, a force sensing load cell, to measure the force exerted between the active member and the remainder of the structure, and a relative position sensing eddy current sensor, to measure the extension of the member/structure, are present in each active member. These active members are high voltage piezoelectric stacks and are driven by high voltage Kaman power amplifiers.

4. Structural Control

Due to the presence of light damping in the truss structure and the noncolocation of the optical set up, design of a robust high bandwidth and high authority optical pathlength compensator is impossible without augmenting structural damping. The frequency response functions (FRF) of voice coil (VC) to the laser pathlength variation are shown in figure 4. The FRF with no structural control (ie, without damping augmentation), represented by the

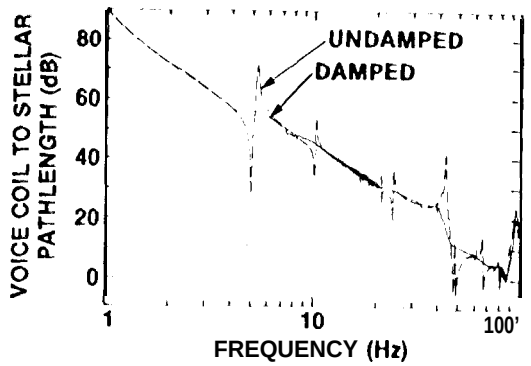

Figure 4: Voice coil to optical pathlength frequency response function before and after structural control

dashed line, contains a large number of very lightly damped modes and some of which are noncolocated. It turned out that a low bandwidth and moderate gain voice coil compensator, that can be designed for the undamped structure with reasonable gain and phase margins, is not adequate to achieve the performance level that is required for maintaining the optical pathlength variation to less than 15 nanometer 1'11)s.

Four passive dampers and four active members are deployed to make the structure quiet and to enhance the damping of the structural modes specially in the neighborhood of a moderately high cross-over frequency of the voice coil controller. The locations of the active ant] passive members are chosen to maximize the energy dissipation of the specific set of modes using the maximum strain energy criterion [6]. Simple co-located integral force feedback (IFF) loops (described below) [7] are closed around the active members to achieve the impedance (defined by the ratio of velocity to force) match [8,9] for an optimum damping performance. Modes at higher frequencies are targeted by the active members because of their tunability. The FRF of voice coil to the laser pathlength for the damped structure (figure 4) and the disturbance transmission function (figure 5) from a disturbance shaker input to the laser pathlength show a significant enhancement of damping for various structural modes for up to 100 Hz. The damping in the major modes has been increased to above 5% of the critical damping from fractions of a percent in the undamped strut.tule.

The concept behind matching impedance of an active member to that of the structure is based on increasing damping for maximum vibrational power

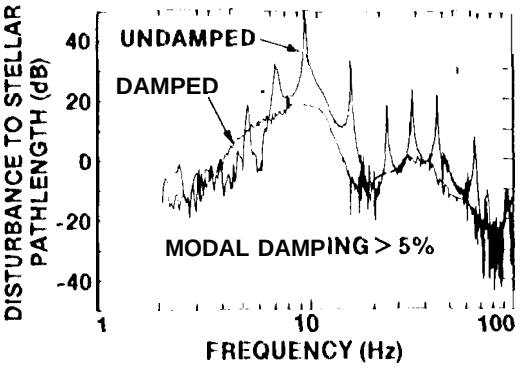

Figure 5: Disturbance attenuation by Structural

('0111101

dissipation. It can be shown that in order to effect a maximum rate of energy dissipation through the active member, the impedance of the active member should be equal to the complex conjugate of the structural impedance Z_{str} s) at the interface point between itself and the active member[4]. Meeting this condition exactly on flexible structures is not practical for two reasons. The first reason is that lightly damped structures contain sharp resonances in their impedance functions that are highly sensitive to perturbations in structural characteristics such as natural frequency. It is extremely difficult to precisely match these resonances. The second reason is that the complex conjugate of the impedance of a structure is a non positive-real function that cannot be approximated over a broad frequency range with stable electrical circuits. Alternatively, if the active member's impedance is made equal (matched) to the smoothed average impedance of the structure, an excellent damping performance is achieved. In this case, poles and zeros of the combination are moved further left in the negative half of the complex plane instead of pushing them towards negetive infinity.

Figure 6 describes a complete integral force feed back control system for enhancing modal damping by matching impedance of an embedded active member to that of the structure at the interface. The area enclosed by the dashed line represents an active member embedded in the structure where voltage $V(s)$ (to drive the active member) is the input and relative position X (s) from eddy current sensor and force $F(s)$ from load cell are the outputs. $Z_0(s)$ is the open loop active member impedance when voltage V(s) is held to a constant bias value. It is es-

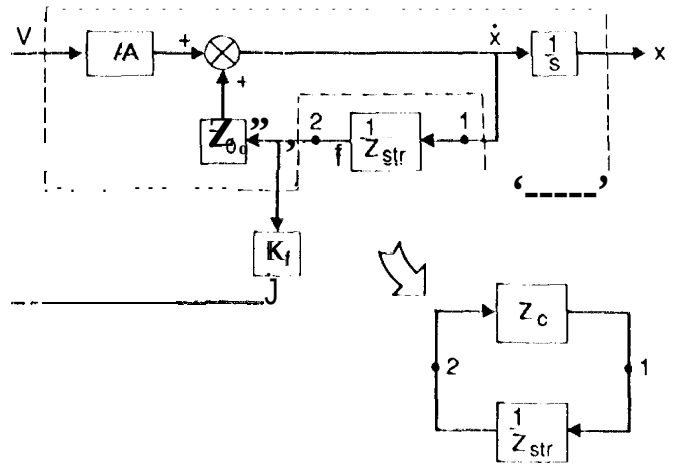

Figure 6: Active damping via Integral Force Feedback (IFF)

sentially a spring with stiffness K_a and impedance

$$Z_0(s) = \frac{s}{K_a}. \quad (1)$$

A(s) is the ratio of velocity $\dot{X}(s)$ to applied voltage $V(s)$ when form $F(s)$ is held to zero and is given by

$$A(s) = K_{am}s, \quad (2)$$

where K_{am} is the active member constant and is related to the stiffness K_a by the following relation

$$K_{am} = \frac{n}{K_a}, \quad (3)$$

where n is linearly proportional to the piezoelectric charge coefficient of the material, number of piezoelectric wafers stacked in the member and the voltage amplifier gain. $Z_{str}(s)$ is the impedance of the structure without the active member as it appears at the interface point of the structure and the member. It is a function of the structural property and the controllability (or equivalently observability) at the interface point and contains all the modes that are colltrc)llable/observable from the interface. The integral force feedback loop is closed through block $K_f(s)$ which is a pure integrator with gain K_I,

$$K_f(s) = \frac{K_I}{s}. \quad (4)$$

The loop transmission from point 2 to point 1 is the active member's closed loop impedance $Z_c(s)$ as it appears to the structure and is depicted in figure

. 6. For an active. member, velocity relates to applied voltage, member's open loop stiffness and imposed force by the following relation

$$\dot{X}(s) = V(s)K_{am}s + F(s)Z_0(s). \qquad (5)$$

The velocity expression is a superposition of two components: the first component is due to applied voltage V(s) and the latter one is due to imposed force $F(s)$. Force $F(s)$ develops due to the fact that the member is embedded into the structure with impedance of $Z_{str}(s)$. For Integral Force Feedback (IFF), the input voltage to the active member has the following form

$$v(s) = F(s)\frac{K_I}{s}. \qquad (6)$$

Substitution of equation 6 into equation 5 yields

$$\dot{X}(s) = F(s)\frac{K_I K_{am}}{s}s + F(s)Z_0(s) = F(s)[K_{am}K_I + Z_0(s)]. \qquad (7)$$

$$Z_c(s) \equiv \frac{\dot{X}(s)}{F(s)} = K_I K_{am} + Z_0(s). \qquad (8)$$

Equations 1 and 3 are substituted into the equation above which yields

$$Z_c(s) = \frac{nK_I}{K_a} + \frac{s}{K_a}. \qquad (9)$$

Equation 9 shows that the closed loop active member, as it appears to the structure, is equivalent to a series combination (figure 7) of a damper and a spring with damping coefficient of $\frac{K_a}{nK_I}$ and spring stiffness of K_a respectively. The problem with this configuration is that it posses no static. stiffness and will accommodate undesirable permanent deformation. However, the stiffness of the member at and near DC can easily be improved by adding a 1st order high pass filter to the compensator. In our experiment a high pass filter with (-3dB) roll off at 1 Hz ($\omega_0 = 6.28$ rads/see) is provided for the load cell of each active member. The resulting $K_f(s)$ is a 1st order low pass filter with pole at $-\omega_0$. The clod loop active member behavior is modified to an elastically coupled damper as depicted in figure 8 and the final impedance is given by

$$Z_c(s) = \frac{1}{\frac{K_a}{nK_I} + \frac{\omega_0 K_a}{nK_I}\frac{1}{s}} + \frac{s}{K_a} \qquad (10)$$

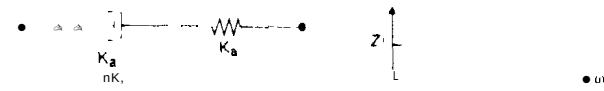

Figure 7: Active member closed loop impedance

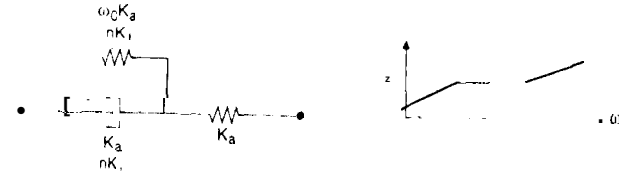

Figure 8: Active member closed loop impedance with high pass filter

The stiffness of the spring parallel to the damper is $\frac{\omega_0 K_a}{nK_I}$. This modification is necessary to recover the static shape of the structure under no-load condition and to void saturation of the integrator and the active member. Finally, an approximate impedance match is obtained by adjusting the value of A'_1. Also, one has the option of modifying the value of ω_0 to improve the match.

The question arises of how the presence of one or multiple closed loop active members in a structure affects stability. Due to the fact that a closed loop active member appears to the structure as $Z_c(s)$ which emulates a passive damper in the frequency range of $\omega > 0$ since $Z_c(j\omega) > 0$ for $\omega > 0$ (figure 9), presence of one or multiple active members in a non-unstable structure do not cause instability in the structure. And coupled with this is the fact that the sensor and actuator of the active member are co-located, stability of the system is robust.

The structural impedance $Z_{str}(s)$ is determined by exciting the structure with the active member, and measuring the ratios of the velocity across the active

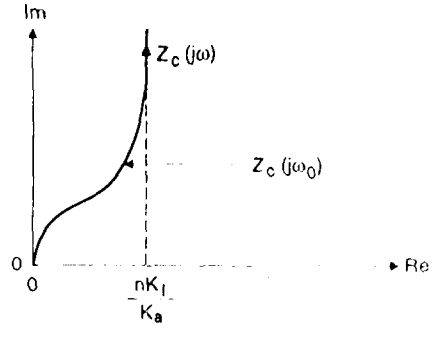

Figure 9: Plot of $Z_c(j\omega), \omega > 0$

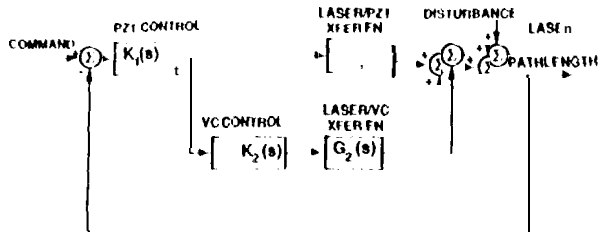

Figure 10: Control system Architecture

member to the force exerted by it. The impedance $Z_0(s)$ of the active member without feedback is obtained by exciting the structure with a disturbance source (a shaker) attached to the structure, and measuring the ratio of velocity to the force at the active member.

5. Direct Pathlength Control

The direct pathlength control (or optical delay line control) is designed to provide coarse (millimeter) to very fine (nanometer) pathlength compensation over a wide frequency bandwidth. The coarse and fine compensations are provided respectively by the voice coil and the PZT actuators that are present in the delay line.

The architecture of this two input (voice coil and PZT) and one output (pathlength) control system is shown in figure 10. Use of a similar architecture in pathlength control experiments has been reported in references [2,3,10]. $G_1(s)$ and $G_2(s)$ are the transfer functions respectively from PZT and voice coil to the pathlength, and $K_1(s)$ and $K_2(s)$ are the compensators respectively for the PZT and the voice coil actuators. Note that the output of the PZT controller ($K_1(s)$) drives both the PZT actuator and the voice coil controller ($K_2(s)$). The open loop transfer function for the system with the given architecture is

$$L = K_1(G_1 + K_2G_2) \qquad (11)$$

The objective is to design the two compensators $K_1(s)$ and $K_2(s)$ such that the closed loop system is stable with adequate gain and phase margins, and the total loop gain $|L(j\omega)|$ is large over the largest achievable bandwidth since the disturbance rejection is proportional to $|L|$ when $|L|$ is large. The following properties are observed from equation (1):

$$L \approx K_1K_2G_2 \quad \text{when } K_2G_2 \gg 1 \qquad (12)$$

$$L \approx K_1G_1 \quad \text{when } K_2G_2 \ll 1 \qquad (13)$$

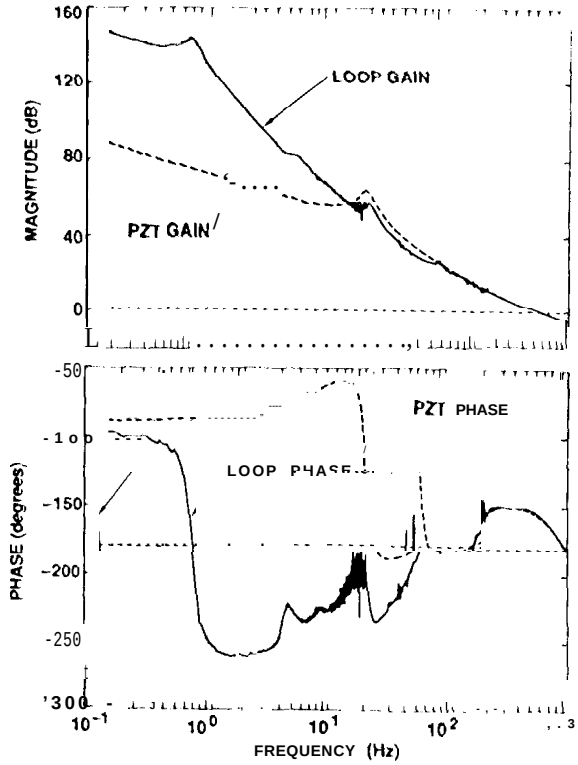

Figure 11: Bode plot of optical control

At low frequency where the voice coil loop gain is large, the total loop gain is equal to the product of the voice coil loop and the PZT compensator gains. At high frequency, the total loop gain approaches the PZT loop gain as the voice coil loop gain approaches zero. As a result, at low frequencies where the pathlength variation is normally large, the voice coil forward loop ($K_2(s)G_2(s)$) being dominant prevents the limited stroke length PZT actuator from saturation. At high frequencies where the pathlength variation is smaller, the PZT forward loop ($K_1(s)G_1(s)$) is dominant and relieves the limited frequency bandwidth voice coil. Bode's classical control design methods [11] are used to design compensators $K_1(s)$ and $K_2(s)$ to shape the open loop system in the frequency domain. This design methodology, unlike mode.m control design methods, does not require an explicit parametric model of the plant but rather uses the measured frequency response functions to synthesize the compensators. With the classical technique, the smooth blending of the two controllers having authorities at two different frequency ranges is simpler than it would be, if possible', with modern control design methodology. Controllers are designed one loop at a time.

The voice coil controller is designed to stabilize the system assuming that it is driven by the pathlength measurement and the the PZT actuator is disconnected. The controller is an 8th order filter including a 2nd order lead filter to provide adequate phase margin at the cross-over frequency (approx. 35 Hz) followed by seven 2nd order notch filters (-3 dB) to provide additional gain margin over 7 local modes at the high frequencies.

The controller for the PZT consists of a first order lag filter and a second order low pass filter. The lag filter provides a high gain at low frequency for good disturbance rejection and the low-pass filter provides at high frequency a -20 dB/dec steep gain roll off with an adequate phase margin for stable control structure interactions. The PZT control loop bandwidth is limited to approximately 500 Hz due to high frequency noise and digital implementation delay. The Bode plot of the optical control loop gain is shown in figure 11.

Both control laws are discretized using 1)ole-zero mapping with zero padding. The effects of time delays due to the computer implementation and the zero order hole] are incorporated in determining the actual phase margin. The low bandwidth voice coil controller and the high bandwidth PZT controller are implemented at 2000 Hz and 10000 Hz respectively.

6. Experiment

The PZT controller K_1 and the voice coil controller K_2 are implemented respectively in V3E/50MHz and V3E/20MH z single board computers (SBC) with a VME bus interface. A third V30/25MHz single board computer is employed to synchronize the control activity and store the time data for later analysis. All programs are written in C language and utilize VxWorks routines for timing the control loops.

A Tektronix 2630 network analyzer is used to derive all the frequency response functions (FRF). A combination of band limited white noise and sine swept inputs are used to generate the FRFs with high coherence levels. The PZT actuator to the pathlength FRF is fairly unaffected by the flexibility of the structure because the mass of the primary mirror on the PZT actuator is small and the PZT actuator is reaction compensated. The compensation is achieved by installing another PX']' actuator

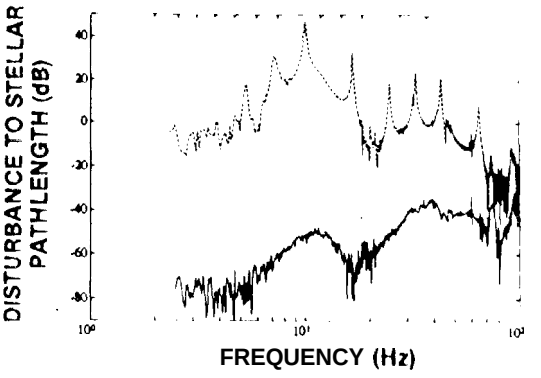

Figure 12: Disturbance attenuation due to structural and optical control

reacting equally in the opposite direction of the control I'Z']' actuator. However a small flexible local mode is present at shout 700" Hz. The phase of the FRF has a slope of -70 μs, while the magnitude is relatively constant. This delay is found to be caused mainly by the time delay of the data transfer from the laser metric system to the analyzer.

The voice coil to the pathlength FRF (figure 4). without structural control is significantly affected by the structural flexibility. The dominant peak at 0.7 Hz (not shown in the figure) is due to the flexure that attaches the trolley to the truss. All other peaks in the FRF correspond to structural modes of the truss. At 80 Hz the phase drops rapidly while modal density and plant uncertainty increases considerably. This lead us to limit the voice coil loop bandwidth to a frequency lower than 80 Hz. Notice that all the modes below 80 Hz in the FRF are not co-located. (Co-located modes arc indicated by alternating poles and zeros,) These noncolocated modes severely limits the bandwidth of the voice coil controller which, along with the 1'7,'1' controller, is unable to maintain the pathlength within the prescribed variation. As mentioned before 4 passive and 4 active dampers are deployed to damp out these noncolocated modes slid a voice coil controller with large bandwidth and adequate stability margin is designed.

The first experiment is carried out to determine the disturbance transmission to the pathlength from a disturbance shaker attached at the mid bay area of the vertical column part of the truss, The dashed line in figure 12 illustrates the disturbance transmission function from the shaker to the pathlength when no structural control (no damping augmentation) and no direct pathlength control are present.

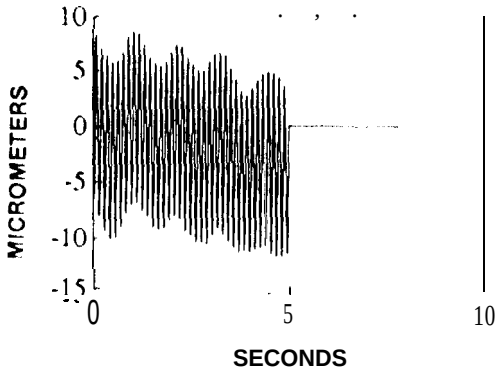

Figure 13: Optical pathlength variation due to resonant excitation (7.3Hz)

One can very easily see the very lightly damped structural resonances in the pathlength output. The solid line in the figure is the transmission function when both structural and direct pathlength controls are deployed. The disturbance rejection is very dramatic ranging from -80dB at the low frequencies to -30 dB at 100 Hz. The bandwidth of the controller is experimentally determined to be approximately 500 Hz. However, as expected, in this region the disturbance attenuation is very low.

Two additional closed loop experiments are carried out the first one is to reject the ambient laboratory disturbances and the second one is to reject a forced resonant disturbance (at 7.3 Hz) induced by the disturbance shaker. in both experiments, after recording open loop pathlength histories for five seconds the control loops are closed and the closed loop pathlength histories are recorded for additional five seconds, The open loop pathlength variation due to the laboratory ambient disturbance has been reduced to 6 nanometer rms from 1.3 micrometer rms a disturbance rejection of -47 dB. A spectral analysis of the open loop and the closed loop data indicates that the achieved bandwidth is approximately 450 Hz and a large part of the closed loop pathlength error is due to the noise at frequencies beyond the controller bandwidth. Figure 13 illustrates the the resonant response experiment. The first five second of the response is clearly dominated by the 7.3 Hz resonant disturbance input to the structure. The closed loop response is down to 8.5 nanometer from .5.6 micrometer a rejection of -57 dB.

7. Conclusion

We have successfully designed and implemented an optical pathlength control system on the JPL phase B flexible testbed for future space optical interferometry. The control designs have! been carried out in the classical frequency domain by directly shaping the measured input output relations, The structural control which enhances the structural damping has enabled the high bandwidth pathlength control for the improved performance. In order to increase the compensation range over a large bandwidth, a smooth handshaking of two controllers having authorities at two different frequency ranges has been effected. Experiments have been carried out to determine the disturbance transmission function and the effective rejection of the laboratory ambient and induced resonant disturbances. The results so far has confirmed that a nanometer level optical pathlength control is feasible in space. It should be mentioned here that the issue of optical wave front tilt control has not been addressed yet and is now a topic of research at JPL.

8. Acknowledgments

This research has been performed at the Jet Propulsion laboratory of the California Institute of Technology under a contract with the National Aeronautics and Space Administration sponsored by the Office of Aeronautics and Space Technology, Code RM. The authors also acknowledge the help of Mike Kantner in designing the post filters and the cooperation of the whole CSI group in completing the experiment.

9. References

1. Laskin, R.A. and San Martin, A., "Control/Structure System Design of a Spaceborne optical Interferometer," AAS/AIAA Astrodynamics Specialist Conference, 1989.

2. O'Neal, M.C. and Spanos, J.T., "Optical pathlength Control in the Nanometer Regime on the JPL Phase B Interferometer Testbed," SPIE International Symposium on Optical Applied Science and Engineering, 1991.

3. Spanos, J.T. and Rahman, Z., "Optical Pathlength Control on the JPL Phase B Interferometer Testbed," 5th NASA/DoD CSI Technology Conference, 1992,

4. Rahman, Z., Spanos, J. and Fanson, J., "Experiments on Active Optical and Structural Con-

trol," 31st IEEE Conference on Decision and Control, 1992

5. Eldred, D.B. and O'Neal, M.C., "The JPL Phase B Testbed Facility," ADPA Active Materials and Adaptive Structures Symposium and Exhibition, 1991.

6. Chu, C.C., Fanson J.L., Milman, M.H. and Eldred, D.B., "Optimal Active Member and Passive Member Placement and Tuning," 4th NASA/DoD Control/Structures Interaction Tech Conference, 1990.

7. O'Brien, J., "Discussion and Experimental Results of Integral Force Feedback for Structural Damping," Interoffice memorandum #354:92:019:JOB, JPL, 1992.

8. Fanson, J.L., Chu, C.C. and Lurie, B. J., "Damping and Structural Control of JPL Phase 0 Testbed Structure," First Joint U. S./Japan Conference on Adaptive Structures, 1990.

9. Chen, G- S., and Lurie, B., "Bridge Feedback for Active Damping Augmentation," AIAA Journal of Guidance and Control, To appear,

10. Colavita, M.M., "Prototype High Speed Optical Delay Line for Stellar Interferometry," SPIE International Symposium on Optical Applied Science and Engineering, 1991.

11. Bode, H.W., Network Analysis and Feedback Amplifier Design, Van Nostrand, NY, 1945.

12. Wilson, J.F. and Davis, L.P., "Viscous Damped Space Structure for Reduced Jitter," 58th Shock and Vibration Symposium, 1987,